

Estimating General Relativity Parameters from Radiometric Tracking of Heliocentric Trajectories

R.S. Park ^{*}, D.J. Scheeres [†], G. Giampieri [‡], J.M. Longuski [§], and E. Fischbach [¶]

Abstract

The theory of GR can be tested by precisely measuring small changes in the trajectory of a spacecraft as it travels near the Sun. An important question is with what accuracy can the relativistic coefficients γ and β be estimated from such a trajectory. We present a detailed covariance analysis of this question, analyzing uncertainties in the spacecraft state and in the GR parameters. The measurement data types simulated in our analysis are range, Very Long Baseline Interferometry (VLBI), and Doppler measurements. Also included are the effects of different phase angles between the Earth and the spacecraft trajectory as well as the realistic error sources. The worst case analysis shows that estimates of these parameters should be obtainable to the order of 0.001 or better, assuming modest improvement in measurement capabilities.

1 Introduction

It has been shown [1] that the Theory of GR can be tested by precisely measuring small changes in the position of a spacecraft as it escapes from the sun on a hyperbolic trajectory. But how well can the relativistic coefficients, also known as the Parameterized Post Newtonian (PPN) parameters, γ and β be estimated from such trajectory (Figure 1)? By forming a state transformation from the initial state and GR parameters to the data measurements, and computing proper partial derivatives, we can estimate the order of accuracy to which we should be able to determine these coefficients, using covariance analysis. A preliminary study based on an analytic approach [2] showed the possibility of measuring the PPN parameters to the order of accuracy 0.001 or better with a foreseeable improvement in spacecraft tracking system (K-band system). This paper presents more detailed numerical analysis including various error sources, such as process noise and station location errors. Also, elliptic orbits are studied to analyze the sensitivity of the uncertainty distribution on the increased data arc and repeated radiometric measurements. The GR effect is at a maximum in the proximity of the Sun and more useful data can be obtained by placing the spacecraft on an elliptic orbit. Moreover, closed orbits allow multiple periapsis passages, which allow increased number of radiometric measurements.

^{*}Ryan S. Park, Department of Aerospace Engineering, The University of Michigan, FXB Building, 1320 Beal Avenue, Ann Arbor, MI 48109-2140, Tel: (734) 834-4878, Fax: (734) 763-0578, sanghp@umich.edu

[†]Daniel J. Scheeres, Department of Aerospace Engineering, The University of Michigan, 3048 FXB Building, 1320 Beal Avenue, Ann Arbor, MI 48109-2140, Tel: (734) 615-3282, Fax: (734) 763-0578, scheeres@umich.edu

[‡]Giacomo Giampieri, Space and Atmospheric Physics, The Blackett Laboratory Imperial College, London, SW7, 2BW, Tel: +44 (0) 20-7594-7775, Fax: +44 (0) 20-7594-7772, g.giampieri@ic.ac.uk

[§]James M. Longuski, School of Aeronautics and Astronautics, Purdue University, 1282 Grissom Hall, West Lafayette, Indiana 47907-1282, Tel: (765) 494-5139, Fax: (765) 494-0307, longuski@ecn.purdue.edu

[¶]Ephraim Fischbach, Physics Department, Purdue University, 525 Northwestern Avenue, West Lafayette, Indiana 47907-2036, Tel: (765) 494-5506, Fax: (765) 494-0706, ephraim@physics.purdue.edu

2 The Transient Effect of γ and β

2.1 General Relativistic Perturbation

The perturbing relativistic acceleration, to first Post-Newtonian (PN) order [3], can be written as:

$$\delta\vec{a} = \frac{m}{r^3} \left[2(\gamma + \beta) \frac{m\vec{r}}{r} - \gamma v^2 \vec{r} + 2(\gamma + 1)(\vec{r} \cdot \vec{v})\vec{v} \right] \quad (1)$$

where \vec{r} and \vec{v} are the spacecraft state vectors and m is the normalized gravitational constant [i.e., $m = (\text{gravitational constant, } \mu)/(\text{speed of light, } c)$]. It can be seen that the relativistic perturbation is present only in the orbital plane. The acceleration components decomposed into the radial R , transverse S , and out-of-plane W directions are:

$$R = \frac{m^2(1 + e \cos f)^2}{a^3(e^2 - 1)^3} [(1 - e^2)\gamma + 2\beta(1 + e \cos f) + 2(\gamma + 1)e^2 \sin^2 f], \quad (2)$$

$$S = \frac{m^2(1 + e \cos f)^2}{a^3(e^2 - 1)^3} [2(\gamma + 1)(1 + e \cos f)e \sin f], \quad (3)$$

$$W = 0. \quad (4)$$

2.2 Hyperbolic Lagrange Equations

The Hyperbolic Lagrange Planetary Equations [6], with proper changes (i.e., $e^2 > 1, a \rightarrow -a$) can be represented as:

$$\frac{da}{dt} = -\frac{2a^{3/2}}{\sqrt{m(e^2 - 1)}} [Re \sin f + S(1 + e \cos f)], \quad (5)$$

$$\frac{de}{dt} = \sqrt{\frac{a(e^2 - 1)}{m}} \left[R \sin f + \frac{S}{e} \left(\frac{p}{r} + \frac{r}{a} \right) \right], \quad (6)$$

$$\frac{di}{dt} = \frac{r}{h} W \cos(\omega + f), \quad (7)$$

$$\frac{d\Omega}{dt} = \frac{r W \sin(\omega + f)}{h \sin i}, \quad (8)$$

$$\frac{d\omega}{dt} = \frac{1}{e} \sqrt{\frac{a(e^2 - 1)}{m}} \left[-R \cos f + S \frac{2 + e \cos f}{1 + e \cos f} \sin f \right] - \frac{d\Omega}{dt} \cos i, \quad (9)$$

$$\frac{dM}{dt} = n - \frac{1}{na} \left[\frac{2r}{a} - \frac{e^2 - 1}{e} \cos f \right] R + \frac{e^2 - 1}{nae} \left[\frac{r}{p} \right] S. \quad (10)$$

where a is semi-major axis, e is eccentricity, i is inclination, ω is argument of perigee, Ω is longitude of ascending node, M is mean anomaly, f is true anomaly, n is mean motion, and F is hyperbolic eccentric anomaly.

After substitution of the perturbing relativistic acceleration components into the Hyperbolic Lagrange Equations [6], the change in the orbital elements from periapsis passage to some value of true anomaly can be approximated by keeping the elements on the right-hand-side constant and varying the true anomaly.

$$\Delta a = \frac{2em}{(e^2 - 1)^2} [(2 + 2\beta + 3\gamma + 2e^2 + \gamma e^2) \Delta \cos f - (2 + \beta + 2\gamma) e \Delta \sin^2 f] \quad (11)$$

$$\Delta e = -\frac{m}{a(e^2 - 1)} [(\gamma + 2\beta + 4e^2 + 3\gamma e^2) \Delta \cos f - (2 + \beta + 2\gamma) e \Delta \sin^2 f] \quad (12)$$

$$\Delta \omega = \frac{m}{a(e^2 - 1)} \left[(2 - \beta + 2\gamma) \Delta f - \left(\frac{2\beta + (1 - e^2)\gamma}{e} \right) \Delta \sin f - (2 + \beta + 2\gamma) \Delta(\sin f \cos f) \right] \quad (13)$$

$$\begin{aligned} \Delta M &= \frac{3m}{a(e^2 - 1)^2} [\gamma + \beta + (2 + \gamma)e^2 + (2 + 3\gamma + 2\beta + (2 + \gamma)e^2)e + (2 + 2\gamma + \beta)e^2] n \Delta t \\ &\quad - \frac{m}{a\sqrt{e^2 - 1}} \left[(2 + 2\gamma + \beta) \Delta(\sin f \cos f) + \frac{\gamma + 2\beta + (4 + 3\gamma)e^2}{e} \Delta \sin f \right] - (2 + \gamma) \frac{m}{a} \Delta F \quad (14) \end{aligned}$$

Figures 2 and 3 show the change in the orbital elements due to the relativistic effect. The initial epoch is at the periapsis with $R_P = 4R_\odot$ and $V_\infty = 39$ km/s, where R_P and R_\odot are the perihelion distance and radius of the Sun, respectively. It is important to note that the largest change in orbital elements occur very early in the trajectory and essentially disappear after a few days.

Of most interest are the partial derivatives of orbital elements with respect to the relativistic constants, γ and β , based on the equations found above. If we let E be the set of orbital elements, a change in E due to relativistic effects can be represented as $E = E_o + \Delta E$, where E_o is the set of initial orbital elements. Taking partials with respect to the GR parameters yields:

$$\frac{\partial E}{\partial(\gamma, \beta)} = \frac{\partial(E_o + \Delta E)}{\partial(\gamma, \beta)} = \frac{\partial \Delta E}{\partial(\gamma, \beta)} \quad (15)$$

The partial derivatives of orbital elements with respect to γ are

$$\frac{\partial a}{\partial \gamma} = -\frac{2em}{(e^2 - 1)^2} [(3 + e^2)(1 - \cos f) + 2e \sin^2 f], \quad (16)$$

$$\frac{\partial e}{\partial \gamma} = \frac{m}{a(e^2 - 1)} [(1 + 3e^2)(1 - \cos f) + 2e \sin^2 f], \quad (17)$$

$$\frac{\partial \omega}{\partial \gamma} = \frac{m}{a(e^2 - 1)} \left[2f - 2 \sin f \cos f + \frac{(e^2 - 1)}{e} \sin f \right], \quad (18)$$

$$\frac{\partial M}{\partial \gamma} = \frac{3m}{a(e^2 - 1)^2} [1 + 3e + 3e^2 + e^3] M - \frac{m}{a\sqrt{e^2 - 1}} \left[2 \sin f \cos f + \frac{(1 + 3e^2)}{e} \sin f \right] - \frac{m}{a} F. \quad (19)$$

The partial derivatives of orbital elements with respect to β are

$$\frac{\partial a}{\partial \beta} = -\frac{2em}{(e^2 - 1)^2} [2(1 - \cos f) + e \sin^2 f], \quad (20)$$

$$\frac{\partial e}{\partial \beta} = \frac{m}{a(e^2 - 1)} [2(1 - \cos f) + e \sin^2 f], \quad (21)$$

$$\frac{\partial \omega}{\partial \beta} = \frac{m}{a(e^2 - 1)} \left[-f - \frac{2 \sin f}{e} - \sin f \cos f \right], \quad (22)$$

$$\frac{\partial M}{\partial \beta} = \frac{3m}{a(e^2 - 1)^2} [1 + 2e + e^2] M - \frac{m}{a\sqrt{e^2 - 1}} \left[\sin f \cos f + \frac{2}{e} \sin f \right]. \quad (23)$$

Figure 4 shows the ratios of the partial derivatives of the orbital elements with respect to the GR parameters as the spacecraft travels on the hyperbolic trajectory. The initial conditions are the same as used above. It is interesting to note that the partials of ω show different behavior between γ and β . This plot clearly shows that there is a possibility of solving for γ and β separately by tracking the spacecraft.

3 The Covariance Analysis and the Least Square Approximation

3.1 Measurement Data Types

For our analysis, three different measurement data types are considered. The first data type is two-way radar range measurement (Z_ρ). This measures the distance between the spacecraft and the tracking station based on the travel time of the uplink and downlink signals. If we let T be signal travel time, the range value $|\rho| \sim 0.5cT$. The second data type we consider is Very Long Baseline Interferometry (VLBI) measurement ($Z_{m,n}$). VLBI measures the longitudinal and latitudinal angles of the spacecraft trajectory in the plane of sky of the tracking station. Combined with range measurements, the 3-dimensional position of the spacecraft can be obtained. The final data type we consider are Doppler measurements, $Z_{\dot{\rho}}$, which measure the frequency shift (Doppler Effect) [7] in the transmitted signals which gives range-rate and, because of the Hamilton-Melbourne effect, provides angular information on the trajectory. Doppler measurements can most simply be represented as range-rate, $\dot{\rho} \approx (\rho_{i+1} - \rho_i)/(t_{i+1} - t_i)$.

3.2 State to be Estimated

At epoch, the spacecraft is located at perihelion ($R_P = 4R_s$) of its heliocentric hyperbolic trajectory with $a_o = 0.58$ AU, $e_o = 1.03$, and $i_o = \omega_o = \Omega_o = M_o = 0$. The trajectories of spacecraft and Earth were assumed to be coplanar and the spacecraft escapes the Sun with $V_\infty = 39$ km/s, which corresponds to periapsis velocity $V_p = 311$ km/s. This nominal trajectory was solved using the following modified Kepler's Equation,

$$\sqrt{\frac{\mu}{|a|^3}}(t - \tau) = e \sinh(F) - F \quad (24)$$

where τ is the periapsis passage time and F is the hyperbolic eccentric anomaly. It is shown [1] that the general relativistic effect is at a maximum when the spacecraft is on a parabolic trajectory. The hypothetical trajectory from Ref. [1] will most likely fly into perihelion as an elliptic orbit and then boost to a hyperbolic escape trajectory. Hence, the above initial state is considered to be the actual condition at epoch. All of these measurement data types are analyzed using a range of different initial phase angles between the Earth and the spacecraft trajectory (i.e., the initial Earth-Sun-spacecraft angle, ϕ , shown in Figure 1.). At epoch for the initial covariance matrix, the conservative initial uncertainties were, $\sigma_x = \sigma_y = \sigma_z = 1$ km, $\sigma_u = \sigma_v = \sigma_w = 1$ m/s, and $\sigma_\gamma = \sigma_\beta = 1$, where σ represents how accurately we know the state components of the spacecraft initially.

3.3 Computation of the Information and Covariance Matrix

Define the function J as follows:

$$J = \frac{1}{2} \sum_i^N \frac{1}{\sigma_i^2} [\bar{Z}_i - Z_i]^2, \quad (25)$$

where N is the number of data measurements, σ_i is the data noise uncertainty, \bar{Z}_i is the actual data measurement, and Z_i is the predicted data measurement. Also, let Y_o be a column vector composed of initial state and GR parameters (i.e., $Y_o = [\vec{r}_o \ \vec{v}_o \ \gamma_o \ \beta_o]^T$). We want to minimize the function J in order to fit the GR parameters to the data. The specific types of data measurement considered were range, VLBI, and Doppler as mentioned earlier. Now minimizing J and linearizing the nominal values of γ and β , we obtain the following expressions.

$$\sum_i^N \frac{1}{\sigma_i^2} (\bar{Z}_i - Z_{i,o}(Y_o)) \left(\frac{\partial Z_i(Y_o)}{\partial Y_o} \right)_o = \left[\sum_i^N \frac{1}{\sigma_i^2} \left(\frac{\partial Z_i(Y_o)}{\partial Y_o} \right)_o \left(\frac{\partial Z_i(Y_o)}{\partial Y_o} \right)_o^T \right] \partial Y_o. \quad (26)$$

where we define the information matrix as

$$\Lambda = \left[\sum_i^N \frac{1}{\sigma_i^2} \left(\frac{\partial Z_i(Y_o)}{\partial Y_o} \right)_o \left(\frac{\partial Z_i(Y_o)}{\partial Y_o} \right)_o^T \right]. \quad (27)$$

The Gaussian Probability Density function is then defined as

$$F(\vec{r}_o, \vec{v}_o, \gamma, \beta) = \frac{\sqrt{\det(\Lambda)}}{16\pi^4} e^{-\frac{1}{2}(Y_o^T \Lambda Y_o)}. \quad (28)$$

The covariance matrix of initial state and GR parameters, P , is then:

$$P = \Lambda^{-1}. \quad (29)$$

4 Model Description

4.1 Partial Derivatives of Data Measurements with respect to State Vector, $\left(\frac{\partial Z}{\partial X}\right)$

Now, we want to analyze the effect of a given initial condition on the GR parameters, and in order to compute the information matrix, Λ , we must first compute the partial derivatives of the measurement partials, $\left(\frac{\partial Z}{\partial X}\right)$, where $X = [\vec{r} \quad \vec{v}]^T$.

The first data type we consider are range measurements,

$$Z_\rho = |\vec{r} - \vec{r}_E - \vec{r}_{TS}| = |\vec{\rho}|, \quad (30)$$

which measure the distance between the spacecraft and the tracking station (TS). Here, \vec{r}_{TS} is the vector representing the location of the Earth tracking station (Goldstone, CA) with origin at Earth center and its analytic representation is

$$\vec{r}_{TS}(t) = \begin{bmatrix} 1 & 0 & 0 \\ 0 & \cos \psi & -\sin \psi \\ 0 & \sin \psi & \cos \psi \end{bmatrix} \cdot \begin{bmatrix} R_E \cos(\alpha + \omega_E t) \sin \delta \\ R_E \sin(\alpha + \omega_E t) \sin \delta \\ R_E \cos \delta \end{bmatrix} = \Psi \cdot \vec{r}_{TS}(0), \quad (31)$$

where ψ is the Earth obliquity (23.45°), R_E is Earth mean radius (6378 km), α is the right ascension (243.17°), and δ is the declination (54.67°). Now, we take the partial derivative of Z_ρ with respect to X to find,

$$\frac{\partial Z_\rho}{\partial X} = \begin{bmatrix} \frac{\partial Z_\rho}{\partial \vec{r}} \\ \frac{\partial Z_\rho}{\partial \vec{v}} \end{bmatrix}^T = \begin{bmatrix} \hat{\rho}(t) \\ 0 \end{bmatrix}_{6 \times 1}^T \quad (32)$$

where $\hat{\rho}$ is the unit position vector of the spacecraft from the Earth tracking station. We consider the precision of the range measurement, σ_i , to range over 10^{-2} , 10^{-3} , and 10^{-4} km.

An alternative data measurement type considered is VLBI, which yields accurate angular measurements of the spacecraft relative to a radio source. We represent this measurement as a set of angles,

$$Z_{(m,n)} = [Z_m \quad Z_n]^T, \quad (33)$$

where Z_m and Z_n are the longitudinal and the latitudinal angular measurements, respectively. Taking partials with respect to X yields,

$$\frac{\partial Z_{(m,n)}}{\partial X} = \begin{bmatrix} \frac{\hat{m}_o^T}{\rho} & 0 \\ \frac{\hat{n}_o^T}{\rho} & 0 \end{bmatrix}_{2 \times 6}, \quad (34)$$

where we define

$$\hat{l}_o = \hat{\rho}, \quad (35)$$

$$\hat{m}_o = \hat{l}_o \times \hat{n}_o, \quad (36)$$

$$\hat{n}_o = \frac{\hat{z} - (\hat{z} \cdot \hat{l}_o)\hat{l}_o}{|\hat{z} - (\hat{z} \cdot \hat{l}_o)\hat{l}_o|}, \quad (37)$$

with $\hat{z} = [0 \quad 0 \quad 1]^T$. ρ is the range from Earth to the spacecraft as we defined earlier. The precision used for the angular measurements were 5, 1, and 0.1 nrad. These angular measurements give us the angular position of the spacecraft.

The final data measurement type we consider is Doppler,

$$Z_D = \frac{d}{dt} |\vec{r} - \vec{r}_E - \vec{r}_{TS}| = \hat{\rho} \cdot \dot{\hat{\rho}}, \quad (38)$$

which is widely used for interplanetary missions. The Doppler measurements measure the shift in frequency due to the Doppler effect, and contains both the range and angular information. The partial derivative of Z_D results in,

$$\frac{\partial Z_D}{\partial X} = \begin{bmatrix} \frac{\partial \hat{\rho}}{\partial \vec{r}} \dot{\hat{\rho}} \\ \hat{\rho} \end{bmatrix}_{6 \times 1}^T, \quad (39)$$

where

$$\frac{\partial \hat{\rho}}{\partial \vec{r}} = \frac{1}{\rho} [I_3 - \hat{\rho} \hat{\rho}^T]. \quad (40)$$

The precision, σ_i , used for the Doppler measurement were 10^{-6} , 10^{-7} , and 10^{-8} km/s.

4.2 Numerical Model Description

Define the state vector as

$$Y = [\vec{r} \quad \vec{v} \quad \gamma \quad \beta]^T. \quad (41)$$

The total time derivative of Y is then expressed as,

$$\dot{Y} = F(Y, \gamma, \beta) = [\dot{\vec{r}} \quad \dot{\vec{v}} \quad \dot{\gamma} \quad \dot{\beta}]^T = [\vec{v} \quad \vec{a} \quad 0 \quad 0]^T, \quad (42)$$

where

$$\vec{a} = -\frac{\mu}{r^3}\vec{r} + \delta\vec{a}. \quad (43)$$

$\delta\vec{a}$ is the relativistic perturbing acceleration given in Section 2 and its non-dimensionalized form is

$$\delta\vec{a} = \frac{\mu}{c^2 r^3} \left[2(\gamma + \beta) \frac{\mu\vec{r}}{r} - \gamma v^2 \vec{r} + 2(\gamma + 1)(\vec{r} \cdot \vec{v})\vec{v} \right]. \quad (44)$$

Now, the measurement partial can be expressed as,

$$\frac{\partial Z}{\partial Y_o} = \frac{\partial Z}{\partial Y} \frac{\partial Y}{\partial Y_o}, \quad (45)$$

where the state transformation matrix, $\Phi = \frac{\partial Y}{\partial Y_o}$,

$$\Phi = \begin{bmatrix} \Phi_{\vec{r}\vec{r}_o} & \Phi_{\vec{r}\vec{v}_o} & \Phi_{\vec{r}(\gamma_o, \beta_o)} \\ \Phi_{\vec{v}\vec{r}_o} & \Phi_{\vec{v}\vec{v}_o} & \Phi_{\vec{v}(\gamma_o, \beta_o)} \\ \Phi_{(\gamma, \beta)\vec{r}_o} & \Phi_{(\gamma, \beta)\vec{v}_o} & \Phi_{(\gamma, \beta)(\gamma_o, \beta_o)} \end{bmatrix} = \begin{bmatrix} \left(\frac{\partial X}{\partial X_o} \right)_{6 \times 6} & \left(\frac{\partial X}{\partial(\gamma, \beta)} \right)_{6 \times 2} \\ 0_{2 \times 6} & I_{2 \times 2} \end{bmatrix}_{8 \times 8}, \quad (46)$$

with $\Phi_o = I_{8 \times 8}$. Now taking the time derivative of the state transformation matrix, Φ , yields,

$$\dot{\Phi} = \begin{bmatrix} \left(\frac{\partial X}{\partial X_o} \right)'_{6 \times 6} & \left(\frac{\partial X}{\partial(\gamma, \beta)} \right)'_{6 \times 2} \\ 0_{2 \times 6} & 0_{2 \times 2} \end{bmatrix}_{8 \times 8}. \quad (47)$$

The superscript ' denotes the total time derivative of a partial derivative matrix. The time derivative of the state partial with respect to initial state yields,

$$\left(\frac{\partial X}{\partial X_o} \right)' = \left(\frac{\partial \dot{X}}{\partial X} \right)_{X(t)} \cdot \left(\frac{\partial X}{\partial X_o} \right) \quad (48)$$

where

$$\left(\frac{\partial \dot{X}}{\partial X} \right)_{X(t)} = \begin{bmatrix} \frac{\partial \vec{v}}{\partial \vec{r}} & \frac{\partial \vec{v}}{\partial \vec{v}} \\ \frac{\partial \vec{a}}{\partial \vec{r}} & \frac{\partial \vec{a}}{\partial \vec{v}} \end{bmatrix} = \begin{bmatrix} 0_{3 \times 3} & I_{3 \times 3} \\ \frac{\partial}{\partial \vec{r}} \left(-\frac{\mu}{r^3} \vec{r} + \delta\vec{a} \right) & \frac{\partial}{\partial \vec{v}} \left(-\frac{\mu}{r^3} \vec{r} + \delta\vec{a} \right) \end{bmatrix}_{6 \times 6}, \quad (49)$$

and the partial with respect to state vectors,

$$\begin{aligned} \frac{\partial}{\partial \vec{r}} \left(-\frac{\mu}{r^3} \vec{r} + \delta\vec{a} \right) &= -\frac{\mu}{r^3} \left[I_{3 \times 3} - \frac{3}{r^2} \vec{r}\vec{r}^T \right] + \frac{2\mu^2(\gamma + \beta)}{c^2 r^4} \left[I_{3 \times 3} - \frac{4}{r^2} \vec{r}\vec{r}^T \right] - \frac{\mu\gamma}{c^2} \frac{(\vec{v} \cdot \vec{v})}{r^3} \left[I_{3 \times 3} - \frac{3}{r^2} \vec{r}\vec{r}^T \right] \\ &\quad + \frac{2\mu(\gamma + 1)}{c^2 r^3} \left[\vec{v}\vec{v}^T - \frac{3}{r^2} (\vec{r} \cdot \vec{v}) \vec{r}\vec{v}^T \right], \end{aligned} \quad (50)$$

$$\frac{\partial}{\partial \vec{v}} \left(-\frac{\mu}{r^3} \vec{r} + \delta\vec{a} \right) = -\frac{2\mu\gamma}{c^2 r^3} \vec{v}\vec{r}^T + \frac{2\mu(\gamma + 1)}{c^2 r^3} \left[\vec{r}\vec{v}^T + I_{3 \times 3} (\vec{r} \cdot \vec{v}) \right]. \quad (51)$$

The time derivative of state partial with respect to the GR paramters can be expressed as,

$$\left(\frac{\partial X}{\partial(\gamma, \beta)}\right)' = \left(\frac{\partial \dot{X}}{\partial X}\right)_{X(t)} \cdot \left(\frac{\partial X}{\partial(\gamma, \beta)}\right) + \frac{\partial \dot{X}}{\partial(\gamma, \beta)}. \quad (52)$$

These partials are defined as:

$$\frac{\partial \dot{X}}{\partial(\gamma, \beta)} = \begin{bmatrix} \frac{\partial \vec{v}}{\partial \gamma} & \frac{\partial \vec{v}}{\partial \beta} \\ \frac{\partial \vec{a}}{\partial \gamma} & \frac{\partial \vec{a}}{\partial \beta} \end{bmatrix} = \begin{bmatrix} 0 & 0 \\ \frac{\partial(\delta \vec{a})}{\partial \gamma} & \frac{\partial(\delta \vec{a})}{\partial \beta} \end{bmatrix}, \quad (53)$$

where

$$\frac{\partial(\delta \vec{a})}{\partial \gamma} = \frac{\mu}{c^2 r^3} \left[\frac{2\mu \vec{r}}{r} - v^2 \vec{r} + 2(\vec{r} \cdot \vec{v}) \vec{v} \right] \quad (54)$$

$$\frac{\partial(\delta \vec{a})}{\partial \beta} = \left[\frac{2\mu^2}{c^2 r^4} \vec{r} \right]. \quad (55)$$

5 Filter Model and Error Sources

5.1 Square Root Information Filter

The inversion of the Information Matrix usually entails loss of numerical precision. The Square Root Information Filter (SRIF) is used to obtain a more numerically precise Covariance Matrix, P . Define

$$\Lambda = R^T R \quad (56)$$

where R is the SRIF Matrix [4]. Let T_H be an orthogonal householder transformation matrix such that

$$T_H \begin{bmatrix} R \\ \frac{\partial Z}{\partial Y_o} \end{bmatrix} = \begin{bmatrix} R' \\ 0 \end{bmatrix}. \quad (57)$$

The updated information matrix is then,

$$\Lambda' = (R')^T (R') \quad (58)$$

and the updated covariance matrix, P' , becomes

$$P' = (\Lambda')^{-1} = (R')^{-1} (R')^{-T}. \quad (59)$$

5.2 Stochastic Acceleration

The effect of time correlated random accelerations can be included in the SRIF matrix based on Ref. [4],

$$\dot{R} = R_o \dot{\Phi}^{-1} = -R_o \Phi^{-1} A = -RA + F(R) \quad (60)$$

where $F(R)$ is the stochastic acceleration given as follows:

$$F(R) = -\frac{1}{2} R B P_\omega B^T R^T R \quad (61)$$

where

$$B = \begin{bmatrix} 0_{3 \times 3} & I_{3 \times 3} & 0_{2 \times 3} \end{bmatrix}^T, \quad (62)$$

$$P_\omega = 2T\sigma_a^2 I_{3 \times 3}. \quad (63)$$

Here, $\sigma_a = 10^{-12}$ km/s² is the steady state acceleration noise and $T = 0.5$ days is the correlation time. Between measurements the SRIF matrix is propagated by solving this differential equation.

5.3 Station Location Error

Define the consider station location vector, \vec{r}_{SL} as,

$$\vec{r}_{SL} = \begin{bmatrix} R_E \sin \delta \\ R_E \cos \delta \\ \alpha \end{bmatrix}. \quad (64)$$

Then taking partials of range measurement with respect to the station location vector results in

$$\frac{\partial Z_\rho}{\partial \vec{r}_{SL}} = -\left(\Psi \frac{\partial \vec{r}_{TS_o}}{\partial \vec{r}_{SL}}\right)^T \hat{\rho} \quad (65)$$

where

$$\frac{\partial \vec{r}_{TS_o}}{\partial \vec{r}_{SL}} = \begin{bmatrix} \cos(\alpha + \omega_E t) & 0 & -R_E \sin(\alpha + \omega_E t) \sin \delta \\ \sin(\alpha + \omega_E t) & 0 & R_E \cos(\alpha + \omega_E t) \sin \delta \\ 0 & 1 & 0 \end{bmatrix}. \quad (66)$$

Taking partials of VLBI measurement with respect to the station location vector yields,

$$\begin{bmatrix} \frac{\partial Z_m}{\partial \vec{r}_{SL}} \\ \frac{\partial Z_n}{\partial \vec{r}_{SL}} \end{bmatrix} = \begin{bmatrix} -\left(\Psi \frac{\partial \vec{r}_{TS_o}}{\partial \vec{r}_{SL}}\right)^T \frac{\hat{m}_o}{\rho} \\ -\left(\Psi \frac{\partial \vec{r}_{TS_o}}{\partial \vec{r}_{SL}}\right)^T \frac{\hat{n}_o}{\rho} \end{bmatrix}. \quad (67)$$

Finally, the partial derivatives of Doppler measurements result in,

$$\frac{\partial Z_D}{\partial \vec{r}_{SL}} = -\frac{1}{\rho} \left(\Psi \frac{\partial \vec{r}_{TS_o}}{\partial \vec{r}_{SL}}\right)^T \left(I_3 - \hat{\rho} \hat{\rho}^T\right)^T \dot{\hat{\rho}} - \left(\Psi \frac{\partial \vec{v}_{TS_o}}{\partial \vec{r}_{SL}}\right)^T \hat{\rho}. \quad (68)$$

5.4 Solar Occultation Effects

When the spacecraft passes in front of or behind the Sun (Figure 5), we cannot obtain radiometric measurements. Since the trajectory originates close to the Sun, this can be an important effect in the early stage of the experiment.

Define,

$$\chi = \cos^{-1} \frac{\vec{\rho} \cdot (-\vec{r}_E)}{\rho r}, \quad (69)$$

where $\vec{\rho} = \vec{r} - \vec{r}_E$.

Then, χ is simply the spacecraft-Earth-Sun angle. Based on the geometry of the Earth and Sun, assuming the Earth is in circular orbit about the Sun, the angle between \vec{r}_E and the tangent vector from center of the Earth to outer radius of the Sun, ξ , can be computed and its value is approximately 0.267° . We assume no measurements are taken if $\chi \leq \xi + 0.5^\circ$ for Doppler and VLBI measurements, and $\chi \leq \xi + 5^\circ$ for Range measurements.

6 Results

6.1 Baseline Results

For our analysis, the trajectory condition given in [1,2] was first verified as the baseline case. The spacecraft was initially located at the periapsis of the heliocentric hyperbolic trajectory with $R_p = 4R_\odot$ and $V_\infty = 39$ km/s. All of the data measurements considered were analyzed with different initial phase angles (ϕ) in order to find the optimum position of the Earth (i.e., phase angle ϕ that gives the most accurate GR estimates).

Figure 6 shows the uncertainties when the Range, VLBI, and Doppler measurements are combined. Current technology can provide noise factors of $\sigma_{i,\rho} = 10^{-3}$ km, $\sigma_{i,\dot{\rho}} = 10^{-7}$ km/s, and $\sigma_{i,(m,n)} = 1$ nrad. These noise factors are directly related to how much information we can obtain from the spacecraft trajectory. In other words, one can simply consider the noise factor as a scaling quantity since the uncertainties are linearly proportional to it. We assume that, in the future, each of these will be decreased by an order of magnitude by adoption of K-band measurement systems. Figure 7 shows the correlations between σ_γ and σ_β (i.e., $\sigma_{\gamma\beta}/\sqrt{\sigma_\gamma\sigma_\beta}$). It can be noticed that the GR parameters become more correlated as the spacecraft moves away from periapsis. This is an indication that we must obtain the maximum number of measurements when in proximity of the Sun to separately estimate γ and β .

NOTE: Range $\sigma_i = \sigma_{i,\rho}$, VLBI $\sigma_i = \sigma_{i,(m,n)}$, and Doppler $\sigma_i = \sigma_{i,\dot{\rho}}$

Table 1: Timespan of 30 days with $\Delta t = 15$ minutes.

N = 2881	σ_γ	σ_β	Worst σ_γ	Worst σ_β
Medium Accuracy	$1.35 \cdot 10^{-4}$	$8.75 \cdot 10^{-4}$	$7.26 \cdot 10^{-3}$	$4.70 \cdot 10^{-2}$
High Accuracy	$1.35 \cdot 10^{-5}$	$8.75 \cdot 10^{-5}$	$7.26 \cdot 10^{-4}$	$4.70 \cdot 10^{-3}$

All of the values of σ_γ and σ_β shown in the above table are the final ones taken at the end of the timespan. ‘‘Medium Accuracy’’ consists of combined measurements with currently provided noise factors, whereas ‘‘High Accuracy’’ consists of combined measurements with values one order of magnitude lower than the ‘‘Medium Accuracy’’ case. The uncertainties σ_γ and σ_β tell us how accurately we can estimate the GR parameters. Two obvious ways to increase the accuracy of these parameters are either taking more measurements or by improving the value of the data noise. It is important to note that the GR parameter γ can be estimated more accurately than β . The worst case estimates are obtained by multiplying the formal uncertainties by \sqrt{N} , where N is the number

of measurements. This shows that some improvements to current measurement technology must be made to estimate γ and β to the proposed order 10^{-3} or better.

Figure 8 shows the uncertainties and correlations when the range, Doppler, and VLBI measurements are combined with different initial phase angles; considering the solar occultation effect. The estimates are taken at the end of a 10 day timespan, and each measurement was updated every 15 minutes. We notice that the uncertainties are relatively sensitive to the initial phase angle, ϕ , which tells that the measurements taken in early stage of the trajectory significantly enhance the overall estimates of GR parameters.

As mentioned earlier, longer data arcs and repeated measurements of a closed orbit may improve results. Figure 9 shows the sensitivity of uncertainties in GR parameters as a function of escape velocity, $V_\infty^2 = -\mu/a$, where negative V_∞ represents orbits with negative orbital energies (i.e., elliptic orbits). This shows that the overall change in the uncertainty distribution is not significant, which means that there is a possibility of conducting this new test of general relativity based on elliptic orbits. An important item to notice is that the estimation of β becomes more accurate as specific orbital energy decreases, whereas the estimate of γ is better off with hyperbolic orbits. Considering the repetition in tracking measurements and increased data arc in the vicinity of Sun, elliptical orbits provide more accurate measurements of γ and β , assuming the spacecraft is capable of enduring multiple close passes of the Sun.

6.2 Effects of Consider Parameters

The effect of stochastic acceleration on the state variables (i.e., position and velocity components) are usually negligible for a short period of time; however, its effect on the GR variables was rather significant. Figures 10 and 11 show how the process noise affects the overall tracking performance. This error alone degraded the covariance of γ and β by an order of magnitude. This with the occultation effect will cause a significant problem in estimating GR parameters as well as separately measuring them. If the steady-state uncertainty, σ_a , decreases by an order of magnitude ($\sigma_a = 0.1 \text{ nm/s}^2$), it will be possible to obtain the desired GR accuracy of 0.001. Figures 10 and 11 also show how exactly we should know the station location to achieve this accuracy. As it can be seen, station location uncertainty less than 0.2 meter will ensure the required accuracy. Fortunately, the current technology provides location uncertainties less than 0.2 meters, and we can disregard the effect of station location error. Figure 12 presents time response of GR estimates when station location error of 0.8, 0.2, and 0.1 meters were considered. This error does not affect the overall result of the uncertainties, but the oscillation of the GR estimates indicates that there is a possibility of estimating the station location errors from this test.

6.3 Comparison of Baseline and Solar Probe Trajectories

At the moment, the most feasible NASA mission to carry out this new test of General Relativity is the Solar Probe mission. The semi-major axis of this mission is approximately 2.6 AU with the periapsis distance of $4R_s$ as before. The Solar Probe will perform a Jupiter gravity assist to obtain required speed and will have the periapsis velocity $V_p \approx 308 \text{ km/s}$, which is slightly less than the baseline case. Figure 13 indicates that the resulting covariance in GR parameters, as well as their correlation, will not be degraded by flying in an elliptic orbit. The hyperbolic trajectory provides a slightly better result; however, Solar Probe's multiple perihelion passages will increase the level of accuracy. This indicates that there is a strong possibility in carrying out this new GR experiment as a part of the Solar Probe mission objectives.

7 Conclusions/Future Work

The purpose of this paper was to show the feasibility of carrying out the new, unique test of general relativity proposed in Ref. [1] and [2]. The spacecraft was considered as an idealized particle and we applied covariance analysis to study the uncertainty distributions based on hyperbolic and elliptic orbits. Also, various error sources were included to study their impact on the overall performance of uncertainty dynamics. Although this is a preliminary-level analysis, it captures most of the fundamentals for performing the actual experiment. Several crucial characteristics of uncertainties in PPN parameters were obtained from this analysis. The first important fact is that placing a spacecraft on a heliocentric elliptic orbit performs essentially equivalent to a hyperbolic orbit, plus the increased data arc and multiple orbits will enhance the estimation accuracy of these coefficients. This led us to consider carrying out this test as a part of the Solar Probe mission, which is currently under development by NASA. To do so, some improvements in spacecraft tracking technology will be required. The stochastic effect significantly degrades the accuracy of the measurements, and hence, it would be necessary to decrease the steady-state uncertainty, σ_a , to less than 10^{-13} km/s². The station location error does decrease the accuracy of PPN parameters, however, the current technology provides station location error less than 0.2 meters.

Under ideal conditions, we have demonstrated that GR can be tested to unprecedented accuracy by tracking spacecraft trajectories near the Sun. To show the feasibility of an actual experiment we need to perform a more detailed analysis to take into account various nongravitational forces that are known to be important due to solar radiation, solar dust, and solar wind. These disturbances will be addressed in a future work.

8 References

- [1] James M. Longuski, Ephraim Fischbach, and Daniel J. Scheeres, "Deflection of Spacecraft Trajectories as a New Test of General Relativity," *Physical Review Letters*, Vol. 86, No. 14, 2001, pp. 2942-2945.
- [2] James M. Longuski, Ephraim Fischbach, Daniel J. Scheeres, Giacomo Giampieri, and Ryan S. Park, "Measurement of the Deflection of Spacecraft Trajectories as a New Test of General Relativity," *Physical Review Letters* (To be submitted).
- [3] C.M. Will, "Theory and Experiment in Gravitational Physics," Cambridge, 1993.
- [4] D.J. Scheeres, D. Han, Y. Hou "Influence of Unstable Manifolds on Orbit Uncertainty," *Journal of Guidance, Control, and Dynamics*, Vol. 24, No. 3, 2001, pp. 573-585.
- [5] K. D. Mease, J. D. Anderson, L. J. Wood, and L. K. White "Tests of General Relativity Using Starprobe Radio Metric Tracking Data," *Journal of Guidance, Control, and Dynamics*, Vol. 7, No. 1, 1983, pp. 36-44.
- [6] J. Prussing and B. Conway, "Orbital Mechanics," Oxford University Press, Inc. 1993, New York.
- [7] T.W. Hamilton and W.G. Melbourne, "Information Content of a Single Pass of Doppler Data from a Distant Spacecraft," *JPL Space Programs Summary*, Vol. 3, No. 37-39, 1966, pp. 18-23.
- [8] R. A. Brouke, "On the Matrizant of the Two-Body Problem," *Astron. and Astrophys.*, Vol. 6, 1970, pp. 173-182.

9 Figures

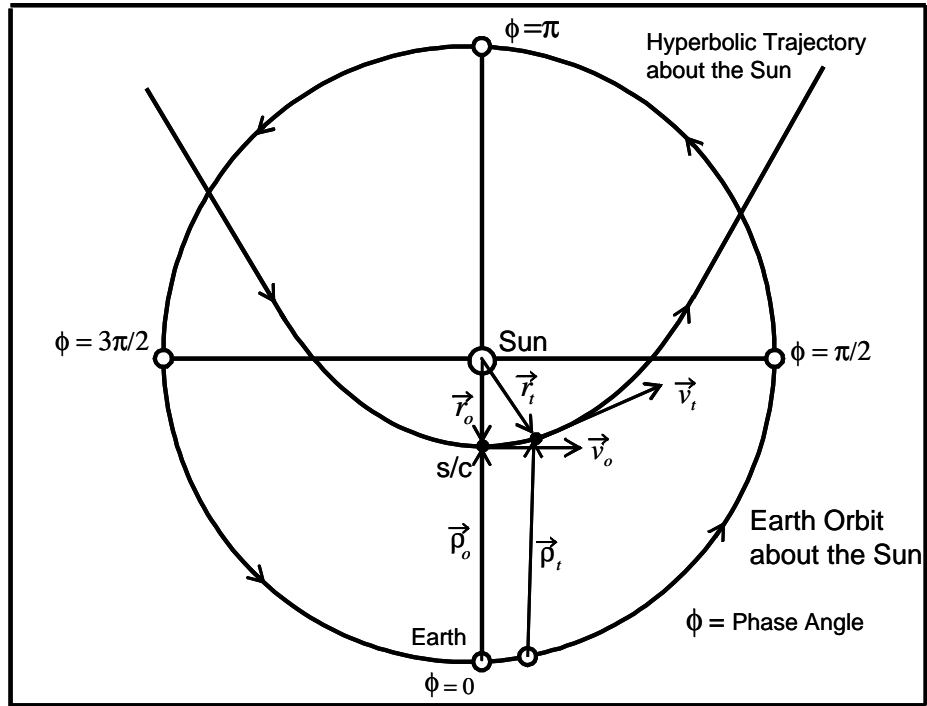


Figure 1: Hyperbolic Flyby of a Spacecraft near the Sun.

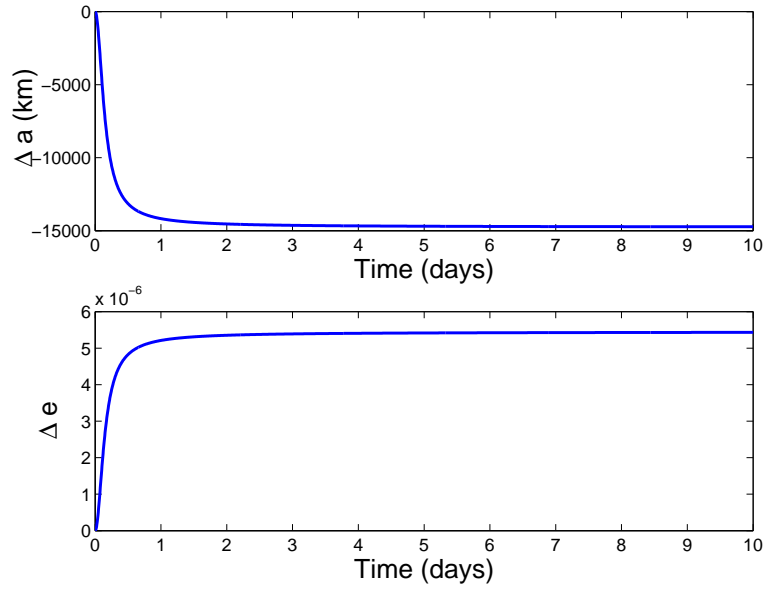


Figure 2: Change in the semi-major axis and eccentricity due to the relativistic effect.

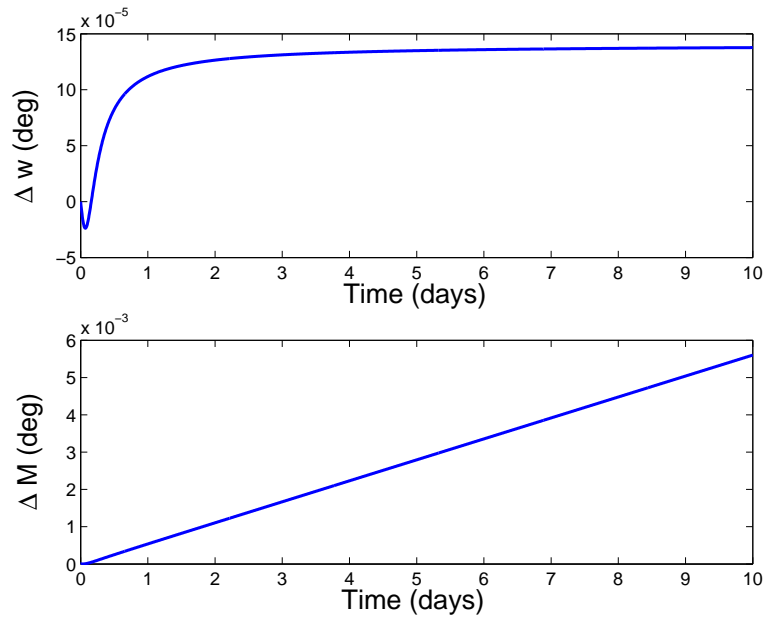


Figure 3: Change in the argument of perigee and mean anomaly due to the relativistic effect.

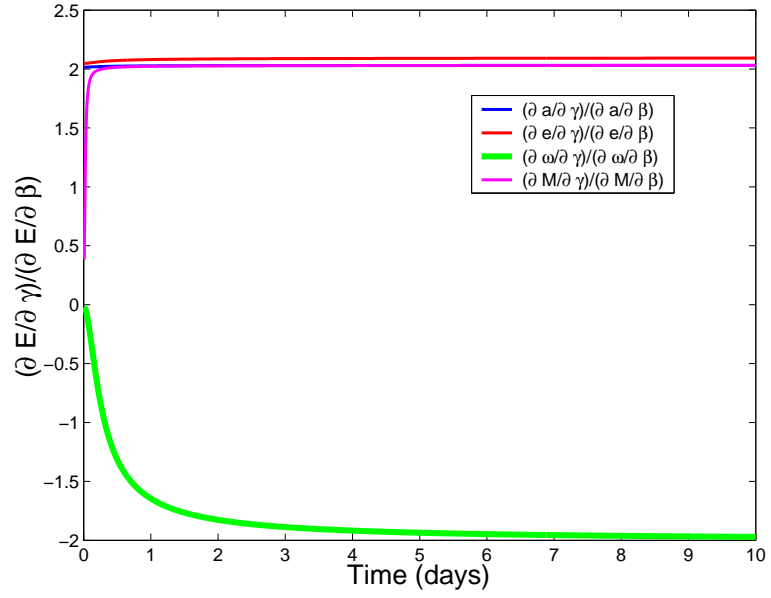


Figure 4: Ratios of orbital element partial derivatives with respect to GR parameters. Time variation of argument of perigee shows the potential to separately estimate γ and β .

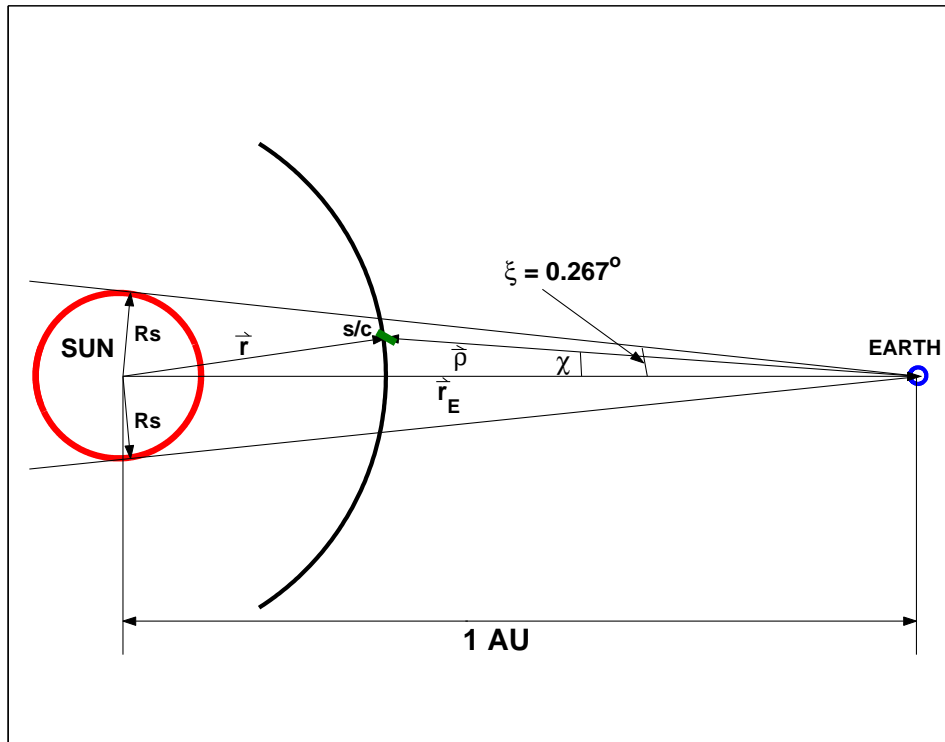


Figure 5: Occultation Effect due to Sun.

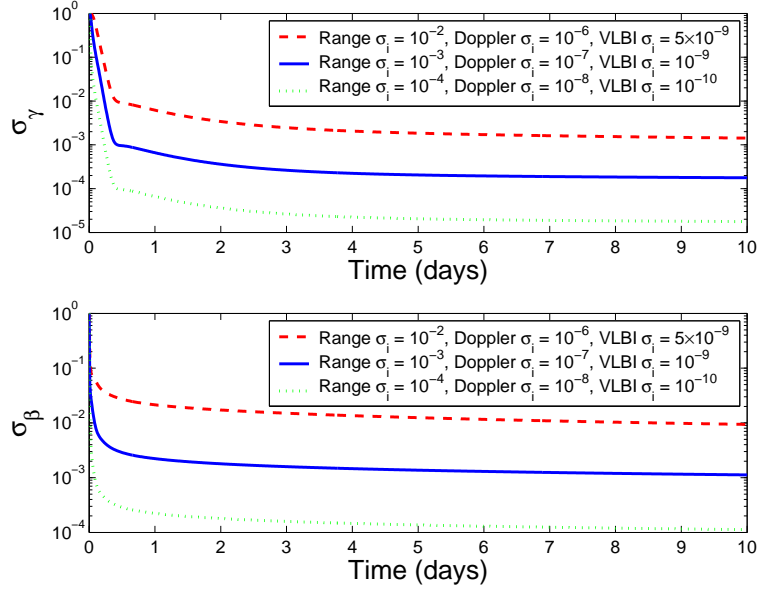


Figure 6: Uncertainties of γ and β measurements as a function of time for different tracking accuracies, σ_i . (No error sources included)

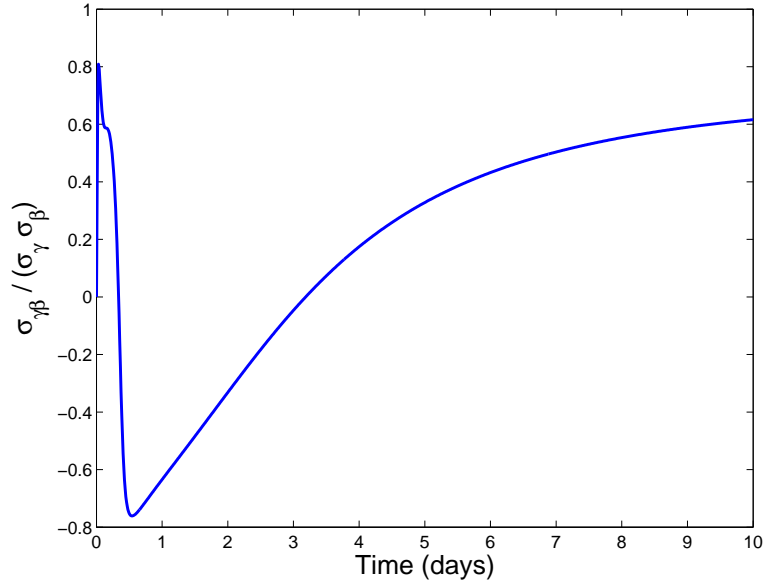


Figure 7: Correlation of γ and β for range, VLBI, and Doppler measurements, with accuracies $\sigma_\rho = 10^{-3}$ km, $\sigma_{m,n} = 10^{-9}$ rad, and $\sigma_{\dot{\rho}} = 10^{-7}$ km/s. (No error sources included)

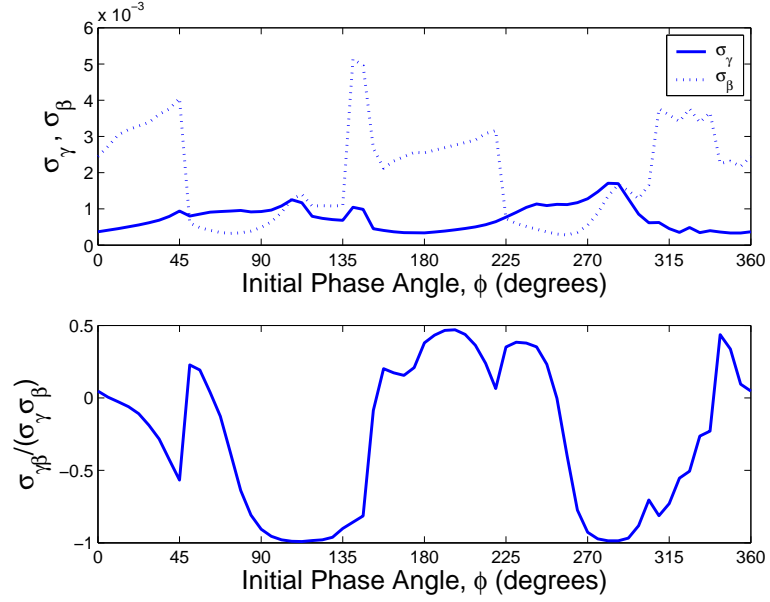


Figure 8: Accuracy and correlation of γ and β estimates as a function of initial phase angle with the Earth. Covariance are taken at the end of 10-day timespan with $\Delta t = 15$ minutes. Range, VLBI, and Doppler measurement accuracies are $\sigma_\rho = 10^{-3}$ km, $\sigma_{m,n} = 10^{-9}$ rad, and $\sigma_{\dot{\rho}} = 10^{-7}$ km/s.

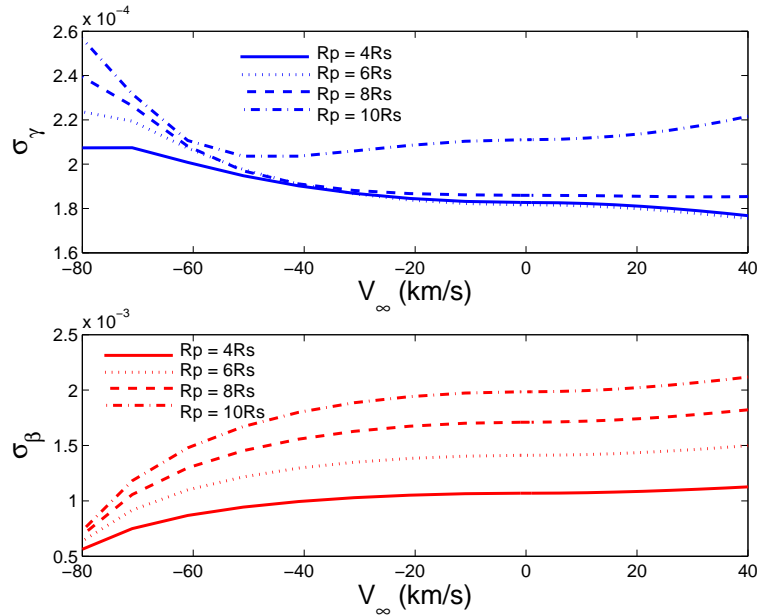


Figure 9: Accuracy of γ and β estimates as a function of escape velocity, V_∞ . Covariance are taken at the end of 10-day timespan with $\Delta t = 15$ minutes. Measurement accuracies are $\sigma_\rho = 10^{-3}$ km, $\sigma_{m,n} = 10^{-9}$ rad, and $\sigma_{\dot{\rho}} = 10^{-7}$ km/s. (No error sources included)

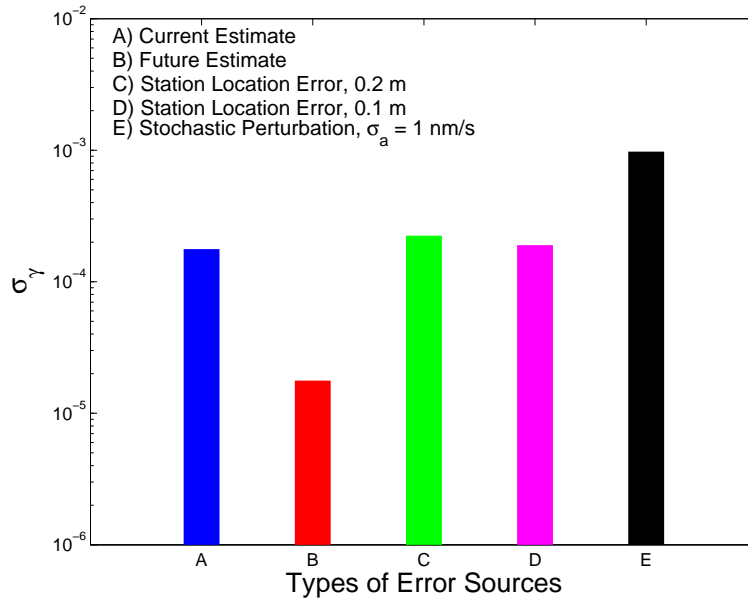


Figure 10: Effect of various errors sources on the accuracy of γ . Estimates are taken at the end of 10-day timespan with $\Delta t = 15$ minutes. Measurement accuracies are $\sigma_\rho = 10^{-3}$ km, $\sigma_{m,n} = 10^{-9}$ rad, and $\sigma_{\dot{\rho}} = 10^{-7}$ km/s.

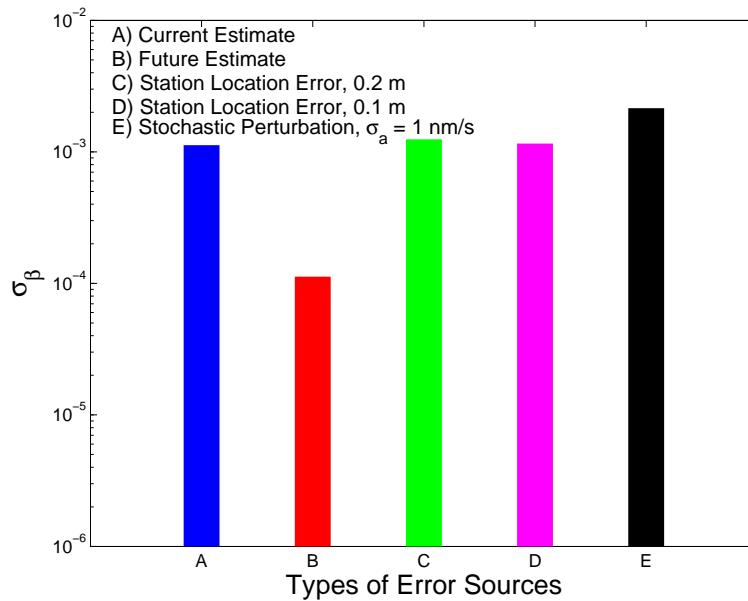


Figure 11: Effect of various errors sources on the accuracy of β . Estimates are taken at the end of 10-day timespan with $\Delta t = 15$ minutes. Measurement accuracies are $\sigma_\rho = 10^{-3}$ km, $\sigma_{m,n} = 10^{-9}$ rad, and $\sigma_{\dot{\rho}} = 10^{-7}$ km/s.

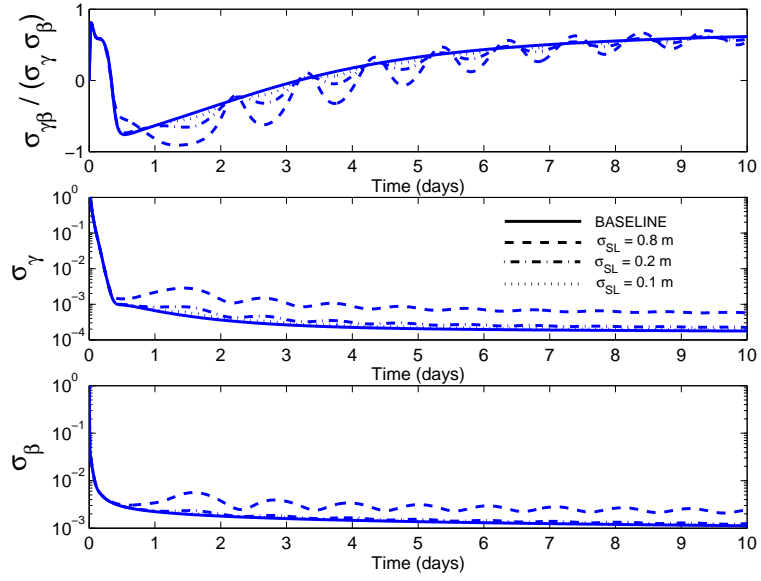


Figure 12: Effect of station location errors on the accuracy of γ and β . Measurement accuracies were $\sigma_\rho = 10^{-3}$ (km), $\sigma_{m,n} = 10^{-9}$ (rad), and $\sigma_{\dot{\rho}} = 10^{-7}$ (km/s) with measurement update for every 15 minutes.

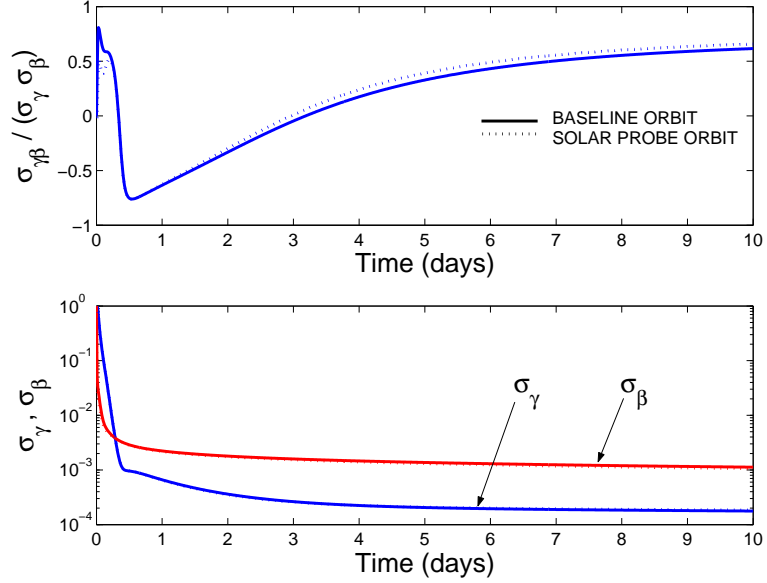


Figure 13: Comparison of GR parameter estimates of baseline and Solar Probe trajectories. Measurement accuracies are $\sigma_\rho = 10^{-3}$ km, $\sigma_{m,n} = 10^{-9}$ rad, and $\sigma_{\dot{\rho}} = 10^{-7}$ km/s with measurement update for every 15 minutes. (No error sources are included)